Infrared spectroscopy of $Li(NH_3)_n$ clusters for $n=4-7$

Tom E. Salter, Victor A. Mikhailov,[a] Corey J. Evans, and Andrew M. Ellis[b]
Department of Chemistry, University of Leicester, University Road, Leicester LE1 7RH, United Kingdom

(Received 4 April 2006; accepted 3 May 2006; published online 17 July 2006)

Infrared spectra of $Li(NH_3)_n$ clusters as a function of size are reported for the first time. Spectra have been recorded in the N–H stretching region for $n=4\rightarrow7$ using a mass-selective photodissociation technique. For the $n=4$ cluster, three distinct IR absorption bands are seen over a relatively narrow region, whereas the larger clusters yield additional features at higher frequencies. *Ab initio* calculations have been carried out in support of these experiments for the specific cases of $n=4$ and 5 for various isomers of these clusters. The bands observed in the spectrum for $Li(NH_3)_4$ can all be attributed to N–H stretching vibrations from solvent molecules in the first solvation shell. The appearance of higher frequency N–H stretching bands for $n\geqslant5$ is assigned to the presence of ammonia molecules located in a second solvent shell. These data provide strong support for previous suggestions, based on gas phase photoionization measurements, that the first solvation shell for $Li(NH_3)_n$ is complete at $n=4$. They are also consistent with neutron diffraction studies of concentrated lithium/liquid ammonia solutions, where $Li(NH_3)_4$ is found to be the basic structural motif. © *2006 American Institute of Physics*. [DOI: 10.1063/1.2208349]

I. INTRODUCTION

The formation of solvated electrons is a well known and widely studied phenomenon in solution chemistry.[1,2] Classic examples of solutions containing solvated electrons are those formed by dissolving alkali metals in liquid ammonia, in which the unpaired valence electron originally on each alkali atom detaches and becomes embedded in the solvent medium. These solutions show properties such as high electrical conductivity and a strong color, which can be directly attributed to the presence of solvated electrons.

Despite numerous investigations, the details of solvated electron formation are not fully understood. Insight can potentially be gained from studies of metal-solvent clusters in the gas phase. Such species may show the onset of properties demonstrated by bulk solutions while still being small enough to be tackled by detailed computational modeling, including quantum chemical calculations. For example, photoionization studies of alkali-ammonia clusters $M(NH_3)_n$, where $M=$Li, Na, or Cs, reveal a dramatic reduction in ionization energies in moving from $n=0$ to 4, with a much slower decline thereafter such that the ionization energy tends towards the bulk ammonia limit (which corresponds to the work function of liquid ammonia).[3–7] These data provide circumstantial evidence for completion of the first solvation shell at $n=4$ and an increased tendency for the unpaired electron on the alkali atom to transfer into the solvent as n increases. However, any attempt to fully explain the properties of the clusters will falter without adequate knowledge of their structures, particularly about the formation of solvent shells around the alkali atom. Spectroscopic techniques provide the key to fully unlock this information.

The spectroscopic study of charged metal-solvent clusters is reasonably well advanced. The advantage of working with charged clusters is that a complete size selection is possible through the use of mass spectrometry prior to photon absorption. Progress in this area has been forged through a combination of this mass selectivity with laser-based spectroscopic techniques. The majority of the work has exploited photodissociation spectroscopy, in which mass-selective detection of one or more ion fragments is measured as a function of laser wavelength, thereby conferring high detection sensitivity. Several research groups have made important and ongoing contributions in this research field. For example, the research groups of Farrar and co-workers,[8–10] Fuke and co-workers,[11–13] Scurlock *et al.*,[14] and Kleiber and co-workers[15–17] have all successfully used electronic photodissociation spectroscopy to probe clusters of singly charged metal atoms (particularly alkaline earth metal cations) with a variety of common laboratory solvents, including water, ammonia, and methanol. Comprehensive summaries of much of this work can be found in two reviews.[18,19]

Infrared photodissociation spectroscopy has recently attracted much attention for probing metal-ion–solvent clusters, since it is a potentially powerful tool for exploring the structural landscape of the electronic ground state. Lisy and co-workers have carried out extensive work on clusters derived from alkali cations, in which a solvent molecule is bound to the cluster rather weakly such that single photon excitation of high frequency vibrations provides enough energy for cluster fragmentation. Solvents such as water,[20,21] methanol,[22] acetone,[23] acetonitrile,[24] and phenol[25] have all been targeted. Duncan[26] and Walker *et al.*[27] have also made major contributions in this area and have broadened the scope of IR photodissociation spectroscopy to include not

[a]Present address: School of Physics, University of Birmingham, Edgbaston, Birmingham B15 2TT, United Kingdom.
[b]Author to whom correspondence should be addressed. Fax: +44 (0)116 252 3789; Electronic mail: andrew.ellis@le.ac.uk

only main group clusters but also the solvation of singly charged transition metal cations. Both single photon absorption and resonance-enhanced IR multiphoton absorption have been used to successfully record photodissociation spectra of these clusters as a function of solvent number. Two recent reviews provide full details of this elegant work.[26,27]

Although singly charged cationic clusters are of great interest, the charge state of the metal ion may not be the one most normally encountered in bulk solutions. This is certainly the case for the alkaline earth cations and it is also the situation for most transition metal ions. To counter this, techniques have been developed in recent years for producing multiply charged cluster ions. For example, Stace and co-workers have recently developed a pickup technique for producing clusters based on multiply charged metal ions.[28,29] Applications of this technique have included the successful recording of photodissociation spectra of the doubly charged cluster ions $[Ag(pyridine)_4]^{2+}$ and $[Cu(pyridine)_4]^{2+}$.[30] However, these developments notwithstanding, the majority of spectroscopic work to date has focused on singly charged metal-solvent cluster cations.

An alternative approach to studying the solvation of ions is to focus on clusters where both cation and anion are present. The study of these uncharged clusters presents very different challenges from charged clusters. In the case of metal-solvent clusters, the issue of singly versus multiply charged ions is avoided, since the metal solute will adopt the charge state dictated by the solvent, which in the limit of a large number of solvent molecules should tally with the charge state in the bulk solution. However, the lack of an overall charge means it is not possible to mass select a particular sized cluster in advance of spectroscopic excitation. As a consequence, spectroscopic studies of neutral solute-solvent clusters have received much less attention than those of charged species.

In the specific case of metal-ammonia complexes in the gas phase, the focus of the present investigation, the work to date has been restricted almost entirely to clusters with one or two ammonia molecules attached to the metal atom. Resonance-enhanced multiphoton ionization (REMPI) spectra of both $AgNH_3$ and $Ag(NH_3)_2$ have recently been recorded.[31–33] Schulz and co-workers have used REMPI to observe the electronic spectrum of $NaNH_3$,[34,35] but larger $Na(NH_3)_n$ clusters do not appear to yield observable electronic spectra by this route. An alternative means of recording absorption spectra of $Na(NH_3)_n$ has been demonstrated by the same group, the use of a photodissociation technique.[36] In this approach single photon absorption of a pulsed ultraviolet laser beam is used to photoionize a range of clusters. A second, tunable pulsed laser is added prior to the photoionization laser pulse, and any absorption of the tunable laser beam is registered as signal depletion in a particular ion mass channel. The assumption here is that the absorption process leads to photodissociation, thus preventing some clusters from being photoionized a short time later. This technique has been used to track the progressive shift of the first electronic absorption band of $Na(NH_3)_n$ from the red ($n=1$) to the near infrared ($n>2$). It was found that at $n=4$ the absorption band had shifted to $\sim 6300\ cm^{-1}$, which is almost identical to the wave number of the solvated electron absorption band in liquid ammonia. Spectra for $n=5$ and $n=6$ yielded essentially the same spectra, the interpretation of which was that the additional ammonia molecules enter a second, more remote solvent shell. The only reports of vibrational spectra for alkali-ammonia cluster have been limited to IR spectra of $LiNH_3$ and $NaNH_3$ trapped in low-temperature argon matrices.[37,38]

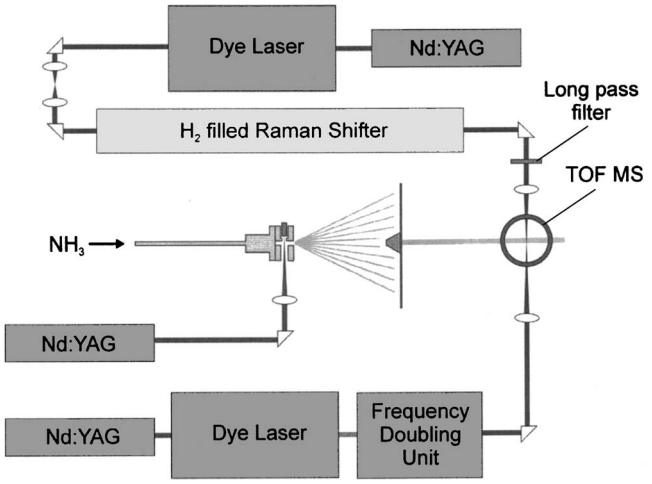

FIG. 1. Schematic view of the experimental apparatus employed in this work. The flight tube of the time-of-flight mass spectrometer (TOF MS) is perpendicular to the plane of the diagram and is therefore not shown.

In this work we report the first mid-infrared spectra of alkali-ammonia clusters for $n>1$. This initial study, the first of several from our laboratory on alkali-solvent clusters, focuses on lithium-ammonia clusters for the case of $n=4-7$. Clusters of this size are likely to span the range of n over which the first solvation shell is completed and the second begins to form. We use a technique similar to the photodissociation technique of Schulz and co-workers described above,[36] but operating in the mid-infrared. Spectra have been recorded in the N–H stretching region, and these have the potential to provide unique structural information about the clusters. To aid the extraction of this information, *ab initio* calculations have been employed in support of the experiments. As will be shown, the combined spectroscopic and theoretical data support the conclusion from ionization energy measurements that the first solvent shell for $Li(NH_3)_n$ is complete at $n=4$.

II. EXPERIMENT

A schematic diagram showing the overall arrangement of the experimental apparatus is presented in Fig. 1. Details of the main features of the experiment are described below.

A. Cluster source

Metal-solvent clusters are produced by reaction of metal atoms with gaseous solvent molecules. The metal atoms were generated by laser ablation using the focused 532 nm output of a small Nd:YAG (yttrium aluminum garnet) laser (Continuum Minilite II). In the experiments described in this paper a static ablation target proved to be satisfactory, but the facility exists for producing alkali metal rods for continuous

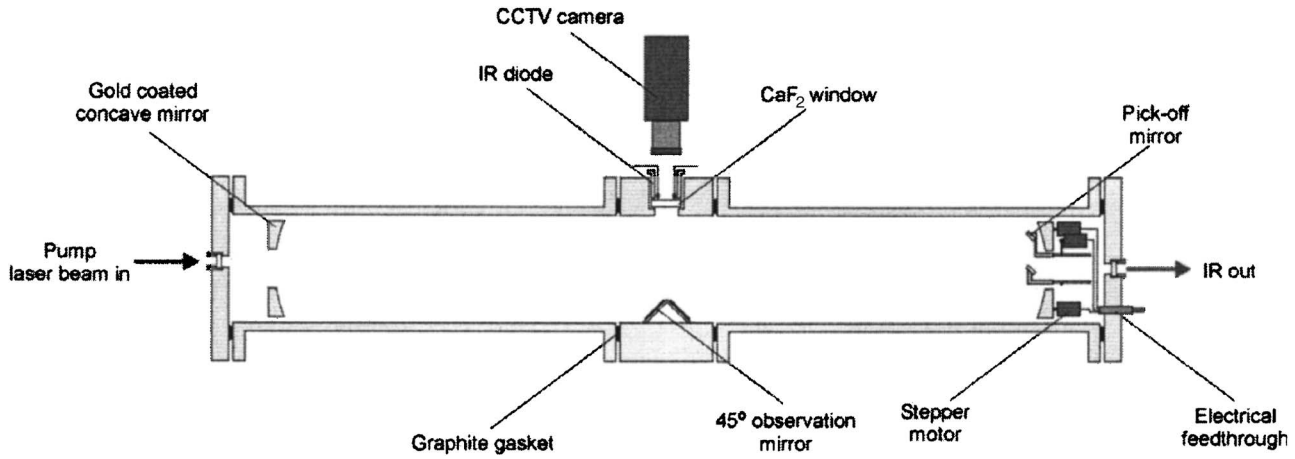

FIG. 2. Schematic view of the homemade Raman shifter.

rotation/translation if desired. In either case the ablation target is made by compressing pieces of lithium at high pressure into an appropriately shaped mold to produce a smooth outer surface. The metal target is then placed inside a standard laser ablation fixture made from aluminum. The fixture is attached to the faceplate of a commercial pulsed valve (Parker Hannifin General Valve, series 9), which provides the source of carrier gas for the experiment. Neat ammonia at a stagnation pressure of 2 bars was employed for most of the experiments described here, rather than a mixture of NH_3 with inert carrier gas, as the former gave the strongest signals for clusters with $n \geqslant 4$.

The pulsed valve was operated at 10 Hz, with an opening time of 250 μs per shot. The firing of the Nd:YAG ablation laser was synchronized with the valve opening and appropriately delayed to ensure that the pulse of gas was over the lithium target as the laser beam hit the metal surface. The resulting gas mixture was then carried along a mixing channel for approximately 5 mm before expanding into a vacuum. The source chamber is pumped by a diffusion pump with a water-cooled baffle operating at an effective pumping speed of $2000\,l\,s^{-1}$. The expanding gas was skimmed several centimeters downstream of the nozzle by a skimmer with a 1 mm orifice and then entered into the mass spectrometer chamber.

B. Time-of-flight mass spectrometer

The time-of-flight mass spectrometer is a homemade system consisting of a linear flight tube of length 1 m and equipped with a dual microchannel plate detector (active surface diameter of 18 mm). The corresponding vacuum chamber is pumped by an $800\ l\ s^{-1}$ turbomolecular pump, which maintains a base pressure of $\leqslant 10^{-6}$ mbar when under full gas load. Laser beams can enter into the region between the repeller and central grid of the Wiley-McLaren ion source through CaF_2 windows (oriented at the Brewster angle) located on both sides of the vacuum chamber.

C. Laser spectroscopy

Infrared spectra were recorded using a two-laser technique. Ions were produced by intersecting the pulsed molecular beam with the frequency doubled output from a pulsed dye laser (Lambda Physik Scanmate 2E pumped by a Continuum Surelite II Nd:YAG laser). The wavelength of this laser was chosen such that the ions could be produced by single photon ionization. For spectroscopic experiments, the UV laser pulse was preceded by the output from a tunable pulsed infrared laser source. To generate tunable infrared radiation, Raman shifting of the visible output from a pulsed dye laser (Sirah Cobra Stretch pumped by a Continuum Surelite I Nd:YAG laser) was employed. Details of the homemade Raman shifter are given later. The spectroscopic technique exploits IR-induced dissociation, which leads to a depletion in the concentration of a cluster of specific size prior to photoionization. In fact, as discussed later, absorption of a single IR photon in the N–H stretching region is not expected to introduce sufficient energy to cause the loss of one NH_3 molecule from small $Li(NH_3)_n$ clusters,[39] where $n \leqslant 3$, but this is possible for larger clusters. When dissociation occurs, depletion of the cluster abundance is registered by a decrease in the corresponding cation signal in the mass spectrometer.

The IR and UV laser beams were directed into the vacuum chamber from opposite directions, and care was taken to ensure that they were spatially overlapped between the repeller plate and the central grid in the mass spectrometer ion source region. Both beams were mildly focused into the chamber and possessed typical pulse energies of 1 mJ for the UV laser and 250 μJ for the IR beam. The delay between the IR and UV pulses was adjusted for optimum signal in each experiment, but was typically set at 50 ns.

The ion signals were captured by a digital oscilloscope and transferred to a PC on a shot-to-shot basis. Gating, averaging, and base line subtraction were all carried out in real time on the PC using bespoke software.

D. Raman shifter

A multipass Raman shifter of the Herriot design was employed for generating tunable IR radiation. A diagram showing key features of the Raman shifter is presented in Fig. 2. The pressure cell is constructed from stainless steel and has an overall length of 3 m. Inside the pressure cell the

end mirrors are 2.5 m apart and consist of planoconcave gold-coated copper mirrors (Laser Beam Products, UK), each with a diameter of 75 mm and a radius of curvature of 1.3 m. To generate IR output near 3000 cm^{-1}, approximately 25 mJ of red laser light from the dye laser was directed into one end of the Raman cell via a CaF_2 window. To obtain a beam profile as close as possible to Gaussian, the main amplifier cell employed in the dye laser was a capillary cell. Prior to entering the Raman shifter, the beam wave front was shaped using a mode-matching telescope. This procedure matches the radius of curvature of the laser beam wave front to those of the mirrors and was vital to ensure both efficient Stokes conversion and to prevent damage to the mirror surfaces. The latter was avoided because the correct wave front curvature ensures that the focal point for the periodic refocusing of the beam is confined to the center of the cell. The Raman cell was filled with pure hydrogen at a typical pressure of 20 bars.

To achieve optimum alignment, one of the internal mirrors was equipped with tilting stages to allow two-dimensional (2D) angle control. Rather than be driven manually by connections to the exterior of the cell, the mirror motion was driven internally by motors mounted inside the Raman cell in combination with a belt-and-pulley system. These high-torque stepper motors (Phytron, UK) were designed for specialized use at high pressures and mild baking conditions. To allow safe alignment, the laser spots on the end mirrors were viewed remotely by a TV camera/monitor combination. The aim in tweaking the end mirror orientation was to ensure that the spots were distributed evenly around both end mirrors. The precise number of laser passes can be chosen by the operator. A small pickoff mirror (also gold coated) is located in front of one of the end mirrors. This can be rotated, also under motorized control, to intercept any of the beams reflecting off the end mirror. For generating third Stokes radiation near 3 μm, we normally use 19 passes. The pickoff mirror sends the beam out through a hole in the center of the end mirror and out of the cell through a CaF_2 window.

The output from the Raman cell contains unconverted dye laser fundamental radiation, as well as unwanted Stokes and anti-Stokes components. The desired third Stokes radiation is separated from other components using an antireflection coated silicon filter prior to being focused into the mass spectrometer vacuum chamber. An upper limit of 0.5 cm^{-1} for the linewidth of the IR radiation has been deduced from the measurement of the photoacoustic spectrum of ammonia in a gas cell in the N–H stretching region.

III. COMPUTATIONAL DETAILS

Calculations were carried out using both density functional theory (DFT) and Møller-Plesset perturbation theory to second order (MP2), as implemented in GAUSSIAN 03.[40] For the DFT calculations the B3LYP functional was used, and for both MP2 and DFT calculations the basis set chosen was 6-311++G(d,p). We have recently carried out high quality *ab initio* calculations on $LiNH_3$ and $Li(NH_3)_2$, in part to "calibrate" DFT calculations against benchmark large basis set MP2 and CCSD(T) results.[39] It was found that the DFT-B3LYP approach, when coupled with a basis set of triple zeta quality with added polarization and diffuse functions, yields good predictions of equilibrium structures and vibrational frequencies (with suitable scaling), and even provides reasonable estimates of Li–N bond dissociation energies. The basis set in this work differs from the aug-cc-pVTZ basis set used in the work described in Ref. 39. The reason for this difference is that the 6-311++G(d,p) basis set is more computationally efficient than aug-cc-pVTZ, which is important for the large clusters studied in the present work. However, our own benchmarking calculations on small clusters show only small differences between the results from calculations performed using 6-311++G(d,p) and aug-cc-pVTZ basis sets.

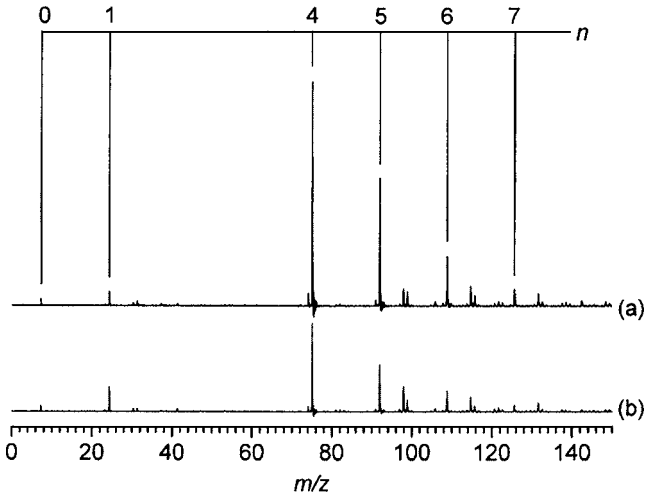

FIG. 3. Mass spectra recorded for (a) IR laser off and (b) IR laser on. The UV laser was fixed at 409.5 nm and the IR laser at 3170 cm^{-1}. The two spectra were recorded on exactly the same vertical scale, so spectrum (b) shows around 60% depletion in all $Li(NH_3)_n^+$ channels ($n \geq 4$) at the chosen IR wavelength.

To find minima on the potential energy surfaces, a trial-and-error approach was employed in which conformations were first sought using low-level calculations, specifically DFT calculations using a minimal (STO-3G) basis set. Having found a minimum, the calculations were then refined using the full basis set. In some cases this led to a minimum also being located in the higher-level calculations, but in other cases the minimum disappeared. All minima were checked to establish that they were not transition states using vibrational frequency calculations. This procedure was repeated for a wide variety of starting configurations in an attempt to find as many minima as possible. To confirm the relative energies of all isomers, the geometry optimizations were repeated with MP2 calculations starting from the structure established from the DFT calculations.

IV. RESULTS AND DISCUSSION

A. Mass spectrometry

A typical mass spectrum in the absence of the IR laser pulse is shown in Fig. 3(a). The photoionization thresholds for $Li(NH_3)_n$ clusters have been measured previously, and it has been found that the thresholds decline as n increases,

with this decline being particularly marked from $n=1 \rightarrow 4$.[3–7] The UV wavelength for the mass spectrum in Fig. 3(a) was 409.5 nm, at which only clusters with $n \geqslant 4$ are expected to be ionized by single photon absorption. Consistent with this expectation, negligible signals are seen for $n=2$ and 3, although there is some residual signal in the $n=1$ mass channel. The $n=1$ signal, coupled with a weak peak due to Li^+, is assumed to be the result of a small amount of two-photon ionization. The dominant signal in the mass spectrum is for $n=4$, with progressively weaker contributions up to $n=7$, beyond which the ion signal becomes negligibly small.

Ion fragmentation is expected to be negligible in the photoionization of alkali-ammonia clusters, given the dominance of diagonal and near-diagonal Franck-Condon factors, as shown in previous photoionization studies.[3–7] Consequently, the ion signal in a given mass channel should reflect the abundance of the neutral cluster at the same mass.

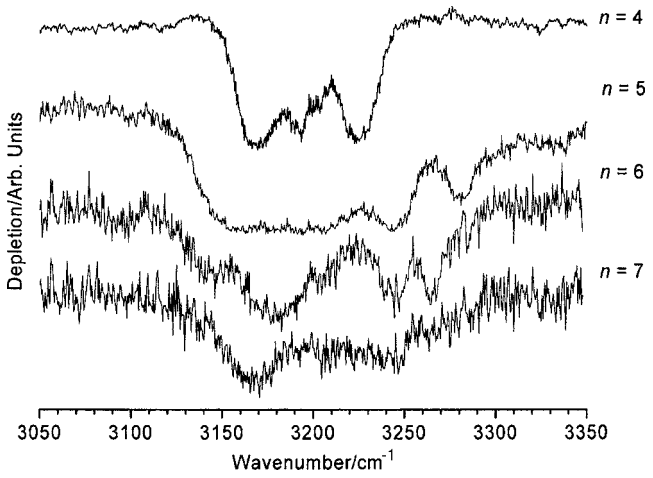

FIG. 4. Infrared spectra of $Li(NH_3)_n$ for $n=4-7$. These spectra have been recorded in ion depletion mode, hence the negative-going peaks.

B. Infrared spectroscopy

IR spectra were recorded for each cluster size by measuring the ion signal depletion as a function of IR laser wavelength in the desired mass channel. The effect of this depletion process is illustrated in Fig. 3(b), in which the IR laser pulse ($3170\ cm^{-1}$) was added just prior to the UV photoionization pulse. As will be seen below, this IR wavelength is resonant with vibrational transitions in several clusters. A signal reduction of ~60% is seen in the $n=4-7$ channels, which is a relatively large effect. Attempts to observe depletion in the $n=1-3$ channels by operating at much shorter photoionization laser wavelengths yielded no detectable depletion for these clusters. The absence of IR photodissociation spectra for $n=1-3$ is assumed to be due to the relatively large Li–N binding energies for these clusters, which prevent IR absorption from causing any cluster fragmentation. It appears that ammonia molecules are more weakly bound in larger clusters, as will be discussed again later, which makes it possible to record IR spectra in the N–H stretching region for $n \geqslant 4$ using the photodissociation approach.

IR spectra of $Li(NH_3)_n$ for $n=4-7$ in the N–H stretching region are shown in Fig. 4. It is assumed that the change in ion signal in a particular mass channel contains contributions only from depletion of the neutral cluster of the same mass. In principle, fragments from IR-induced laser dissociation could complicate the assignment. For example, IR photodissociation of $Li(NH_3)_5$ will lead to formation of $Li(NH_3)_4$, which can then subsequently be photoionized by the UV laser pulse. This process in isolation would lead to an increase in the amount of $Li(NH_3)_4^+$, in contrast to the IR-induced depletion assumed here. This ion production could partly counteract any decrease in ion signal due to photodissociation of $Li(NH_3)_4$, which would in turn distort the IR spectrum. However, these "production" contributions are small. A demonstration of this is provided by the peak at approximately $3280\ cm^{-1}$ seen in the $Li(NH_3)_5$ spectrum, but not seen in the $Li(NH_3)_4$ spectrum. If a sizeable proportion of the $Li(NH_3)_4^+$ ions were the result of IR photodissociation of $Li(NH_3)_5$ followed by UV photoionization, then a positive-going peak in the $n=4$ spectrum should appear at the same wave number. There is no evidence of any such peak above the noise level in this region, suggesting that its contribution is very small. We therefore conclude that any potential confusion from photoionization of IR photodissociation products is negligible. In part this is due to the rather rapid decrease in cluster abundance in going from $n=4 \rightarrow 7$, as seen in the mass spectra in Fig. 3. This monotonic decline in cluster ion intensity aids the separation of IR features from different sized clusters. In addition, the translational energy imparted to ions on photodissociation may lead some to escape from the field of view of the microchannel plate detector, further helping to marginalize ion production signals from photodissociation products. As a result, we consider the IR spectra in Fig. 4 to be clean photodepletion spectra for each cluster size.

Finally, before the spectra of individual clusters are considered, we point out that intramolecular vibrational redistribution (IVR) in these relatively large clusters is assumed to be sufficiently rapid to ensure that IR photodissociation is not vibrational mode selective. The delay between the IR and UV laser pulses has been varied from ~1 ns to several hundred nanoseconds, with no noticeable change in the relative band intensities. This suggests that IVR is complete on the subnanosecond time scale, and, as a result, the IR spectra should accurately profile the IR absorption spectrum for a given cluster in the N–H stretching region.

1. $Li(NH_3)_4$

An enlarged view of the IR spectrum of $Li(NH_3)_4$ is shown in Fig. 5. This spectrum consists of three partly resolved, broad bands spanning a relatively narrow region of $100\ cm^{-1}$ and centered near $3200\ cm^{-1}$. No other bands are discernible above the noise level, and scans over the range of $2600-3500\ cm^{-1}$ have shown no features other than those shown in Fig. 5(a). For comparison, free ammonia shows two N–H stretching fundamentals in its IR spectrum, the symmetric and antisymmetric stretches at 3337 and

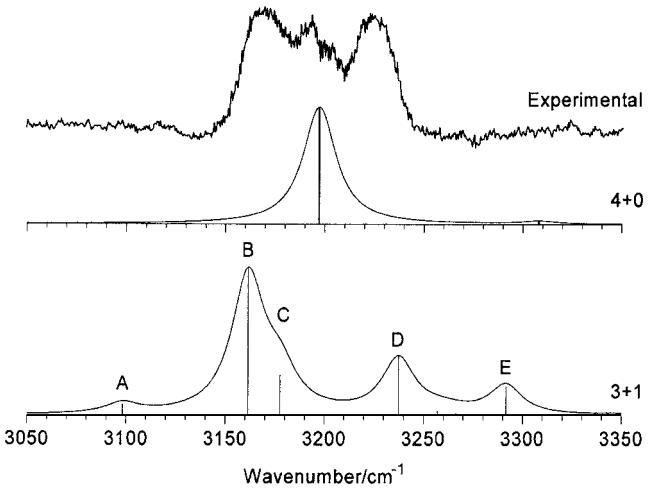

FIG. 5. An enlarged view of the IR spectrum of $Li(NH_3)_4$ in the N–H stretching region is shown in the upper panel. Beneath the experimental spectrum are DFT simulations for the 4+0 and 3+1 conformers. As detailed in the text, the harmonic vibrational frequencies from the DFT calculations have been scaled by a factor of 0.957. The individual vibrational transitions have been convoluted with Gaussian profiles [full width at half maximum (FWHM)=20 cm^{-1}] to generate the simulated spectra above each stick plot.

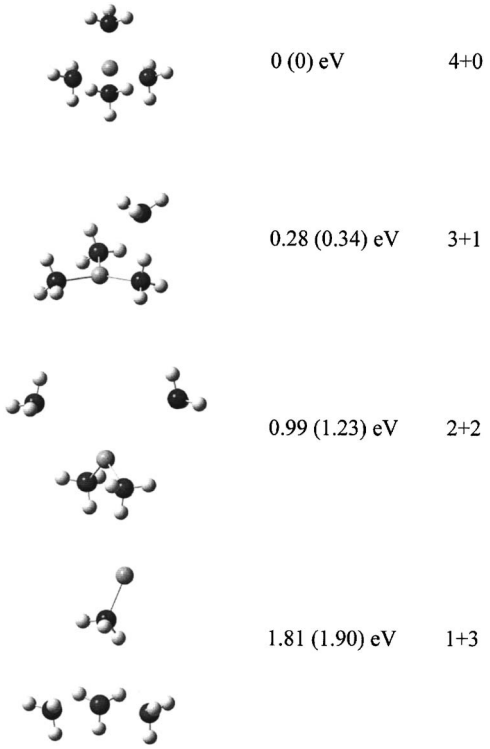

FIG. 6. Calculated isomers of $Li(NH_3)_4$. The relative energies of the isomers are shown and were obtained from DFT and MP2 calculations, the latter being shown in parentheses. See text (Sec. III) for further details.

3444 cm^{-1}, respectively. Consequently, the N–H stretching bands for $Li(NH_3)_4$ show a marked redshift relative to the N–H stretches of NH_3.

DFT and MP2 calculations were employed to aid the spectral assignment.[41] The only previously published *ab initio* calculations on $Li(NH_3)_4$, that by Mierzwicki and Latajka,[42] did not provide vibrational frequency predictions and IR transition strengths. The first step in this part of the study was to identify the likely isomers for this cluster using DFT. Four distinct equilibrium structures were identified in these calculations, as illustrated in Fig. 6. The energy ordering of these isomers was determined using both DFT and MP2 calculations, with relative energies being shown in Fig. 6. The lowest energy isomer is found to consist of four ammonia molecules in a tetrahedral arrangement around the Li atom, each NH_3 molecule being coordinated to Li via the N atom. We use the notation 4+0 to refer to this cluster, where the 4 and 0 refer to the number of solvent molecules in the first and second solvent shells, respectively. The DFT calculations by Mierzwicki and Latajka also found this isomer to be the lowest in energy. Furthermore, previous *ab initio* calculations on $Na(NH_3)_4$ similarly found a tetrahedral structure to be the most stable.[43] In the other, higher energy, isomers, the ammonia molecules can be separated into first and second solvation shell molecules. Thus the second lowest energy isomer has three ammonia molecules in the inner solvation shell and one in the outer shell. We refer to this as the 3+1 isomer. The outer shell NH_3 is hydrogen bonded to a specific inner shell NH_3, rather than "shared" between two or all three inner shell ammonia molecules. The two remaining isomers, the 2+2 and 1+3 isomers, possess much higher energies and are likely to make a negligible contribution to the spectra described here.

Vibrational frequencies and IR transition line strengths have been obtained for all four isomers from the DFT calculations. For comparison with experiment the calculated N–H harmonic stretching frequencies for the clusters have been scaled by 0.957, a multiplier chosen to bring the DFT frequencies of NH_3 into best agreement with the known N–H stretching fundamental frequencies of this molecule. The DFT calculations predict a strong redshift of the N–H stretching vibrational frequencies of ammonia molecules in the inner solvation shell of $Li(NH_3)_4$ when compared with free NH_3. In addition, the calculations predict that the IR absorption strengths for the N–H stretching modes of $Li(NH_3)_4$ are more than two orders of magnitude larger than those in NH_3. Beneath the experimental spectrum in Fig. 5 are simulations based on the DFT results for the 4+0 and 3+1 isomers. Similar findings were obtained for simulations based on MP2 calculations.

The strongest bands in the simulations are close to the observed band positions. However, neither simulation successfully reproduces the entire experimental spectrum, either individually or when superimposed. The simulated spectrum for the 4+0 cluster shows a single strong band accompanied by a very weak feature at higher wave numbers. The strong band is due to excitation of the triply degenerate N–H antisymmetric stretch, the degeneracy arising from the high isomer symmetry. The position of this band in the simulation is close to the center of the experimental band profile. The 3+1 isomer shows more structure in its predicted spectrum, which at first sight is more encouraging, given the added structure in the experimental spectrum. Like that of the 4+0 simulation, the strongest band in the 3+1 simulation falls within the profile of the bands seen in the experimental spectrum. Consequently, one possible assignment of the experimental spectrum is that it contains contributions from both

the 4+0 and 3+1 isomers. However, this ignores the fact that both DFT and MP2 simulations (the latter are not shown here) for the 3+1 isomer show bands with significant intensities spread over a much wider wave number range than seen in the experimental spectrum. In addition, we point out that variations in supersonic expansion conditions, including different stagnation pressures for neat ammonia and also use of ammonia diluted in excess argon carrier gas, produced no changes in relative band intensities in the IR spectrum. Since the 3+1 isomer is calculated to be in the region of 0.30 eV higher in energy than the 4+0 isomer, variations in the degree of cooling produced by different expansion conditions should yield some variation in relative band intensities if both isomers contributed to the spectrum. Consequently, the invariance to expansion conditions is further evidence that the 3+1 isomer does not contribute to the observed spectrum. The 2+2 and 1+3 structures can also be neglected on the basis of their predicted vibrational spectra (not shown here) and the fact that they possess much higher energies than even the 3+1 isomer.

One of the defining features of the 3+1 and 2+2 isomers is the appearance of additional bands of substantial intensity markedly blueshifted from the strongest band in the DFT simulations. These additional peaks arise from excitation of vibrations linked to the presence of an ammonia molecule in the second solvation shell. For example, the highest frequency band in the 3+1 simulation, labeled *E* in Fig. 5, is due to the antisymmetric N–H stretching mode of the ammonia molecule in the inner shell directly hydrogen bonded to the ammonia in the outer solvation shell. Band *D* in the simulation arises from the symmetric N–H stretching vibration of the outer shell ammonia, while bands *B* and *C* are the symmetric N–H stretches, in and out of phase with each other, respectively, arising from the two inner ammonia molecules not directly attached to the outer shell ammonia. Band *A*, the weakest band, is associated with the symmetric N–H stretch of the inner shell ammonia that is hydrogen bonded to the outer shell ammonia. We deduce from this simulation that clusters containing ammonia molecules in more than one solvation shell will show a broad spread of bands, including some further to the blue than those seen in the experimental $Li(NH_3)_4$ spectrum.

The relatively compact structure in the experimental spectrum suggests that all four of the ammonia molecules are located in the inner solvation shell. However, it is also clear that a precise tetrahedral arrangement of the solvent molecules around the central Li atom does not account for the observed spectrum. There are two possible explanations for this discrepancy. One is that we are observing the spectrum of a single, low energy, isomer, but the true symmetry is not fully tetrahedral, leading to loss of some or all of the degeneracy in the N–H stretching vibrations, which could account for the presence of several closely spaced bands. The other alternative is that there are actually several low energy isomers, all based broadly on a single solvation shell occupancy, but with slightly different structures. We have no evidence for either of these two alternatives from our own calculations, but the approximations involved and the limitations of trial-and-error searching for isomers in a potentially complex conformational landscape mean that we cannot rule out either possibility. More sophisticated calculations on $Li(NH_3)_4$ would be very welcome to resolve this matter.

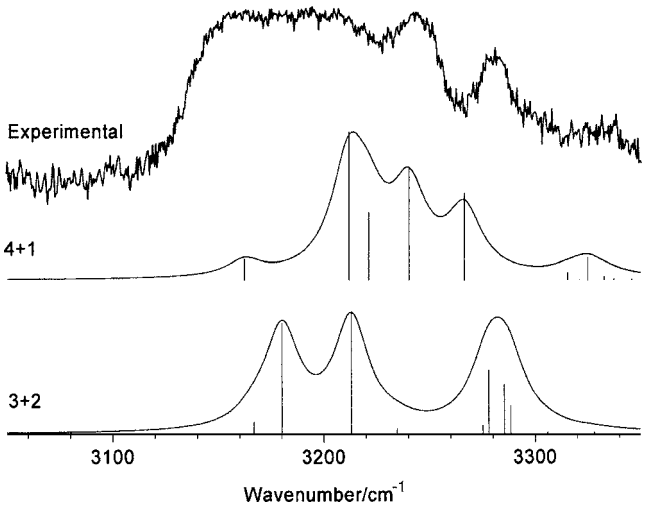

FIG. 7. An enlarged view of the IR spectrum of $Li(NH_3)_5$ in the N–H stretching region is shown in the upper panel. DFT-predicted IR spectra for the 4+1 and 3+2 conformers are shown beneath the experimental spectrum. As detailed in the text, the harmonic vibrational frequencies from the DFT calculations have been scaled by a factor of 0.957. The individual vibrational transitions have been convoluted with Gaussian profiles (FWHM $=20\ cm^{-1}$) to give the simulated spectra above each stick plot.

2. $Li(NH_3)_5$

An enlarged view of the IR spectrum of $Li(NH_3)_5$ is shown in Fig. 7. Three clear features are observed, a very broad band centered at 3175 cm^{-1} and two additional, much narrower bands at 3240 and 3280 cm^{-1}. Based on the discussion earlier for $Li(NH_3)_4$, the first impression conveyed by this spectrum is that the more extensive structure signifies occupation of a second solvation shell in $Li(NH_3)_5$.

As with $Li(NH_3)_4$, attempts have been made to identify the possible isomers of $Li(NH_3)_5$, with the aim of simulating the IR spectrum. Unlike $Li(NH_3)_4$, there have been no previously published *ab initio* calculations on $Li(NH_3)_5$. Four isomers were also found for $Li(NH_3)_5$, with the structures and relative energies shown in Fig. 8. No isomer has been found in which all the ammonia molecules lie roughly in the same solvation shell. As discussed earlier, photoionization measurements of $Li(NH_3)_n$ show a marked discontinuity at $n=4$, which has been interpreted as due to the complete filling of the inner solvation shell.[4–7] Our calculations and our IR spectrum are consistent with this suggestion. The lowest energy isomer can be described as a 4+1 structure, i.e., four ammonia molecules surrounding the Li atom with an additional, and more remote, ammonia molecule in what is effectively a second solvation shell. The three higher energy isomers in Fig. 8 can all be described as 3+2 species, although there are subtle differences in structure in each case. For all the isomers each outer shell NH_3 is hydrogen bonded to a specific inner shell NH_3. Again we emphasize that the isomers in Fig. 8 are those that were found using a simple trial-and-error approach, but other low energy structures may exist.

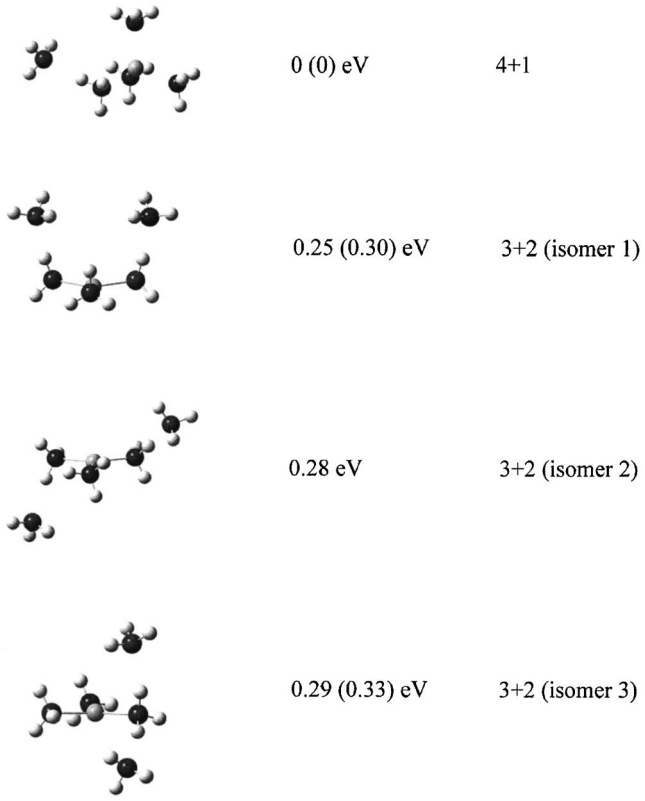

FIG. 8. Calculated isomers of $Li(NH_3)_5$. The relative energies of the isomers were obtained from DFT and MP2 calculations, the latter being shown in parentheses. Calculations on the second highest energy isomer did not converge at the MP2 level, hence only the DFT relative energy is shown.

Simulations of the IR spectra follow the pattern seen for $Li(NH_3)_4$. The strongest bands correspond to N–H stretches of ammonia molecules attached directly to the Li atom and which are not hydrogen bonded to the outer shell ammonia. Further to the blue are bands associated with the outer shell ammonia, which originate from excitation of a N–H stretching vibration in the outer ammonia or N–H stretching vibrations in the inner shell ammonia that is directly hydrogen bonded to the outer shell ammonia. Simulations of the $Li(NH_3)_5$ spectrum based solely on the two calculated lowest energy isomers are shown in the bottom two panels of Fig. 7. Neither simulation matches the experimental spectrum. However, the appearance of well-defined bands on the high wave number side of the spectrum is reproduced, and these bands are clear signatures of the presence of one or more ammonia molecules located in a second solvation shell.

3. $Li(NH_3)_6$ *and* $Li(NH_3)_7$

These two clusters also show the blueshifted features observed for $Li(NH_3)_5$, although in the case of $Li(NH_3)_7$ this blueshifted absorption lacks the clear structure seen for $Li(NH_3)_5$ and $Li(NH_3)_6$. We have not attempted DFT calculations on $Li(NH_3)_6$ and $Li(NH_3)_7$ because of the high cost of such calculations coupled with the expectation of an even more complex structural landscape than found for the smaller clusters. However, we can interpret the spectra by analogy with $Li(NH_3)_5$. The strong bands in the $\sim$3150–3200 cm^{-1} region are assigned to absorption by inner shell ammonia molecules, while the features further to the blue are assigned to the presence of ammonia molecules in an outer solvation shell. The lack of resolved features in the case of $Li(NH_3)_7$ is compounded by the low signal intensity for this cluster, but it may also be the result of contributions from several different isomers, thus smearing out any potential structure.

C. Solvent shell formation

The IR spectra presented here show that, in the gas phase, the first solvation shell for $Li(NH_3)_n$ clusters is full at $n=4$. A criticism sometimes leveled at studies of small clusters is that the findings often bear little relationship to the corresponding bulk material. It is therefore interesting to compare our findings with structural studies of lithium-ammonia solutions.

It has long been suggested that the primary solvation shell in bulk lithium-ammonia solutions contains four ammonia molecules. However, only the most recent structural studies based on neutron diffraction measurements provide a firm confirmation of this picture.[44,45] Wasse and co-workers have obtained structural information from neutron diffraction for solutions of different concentrations. Saturated solutions of lithium in ammonia contain 21 mol % of lithium, which corresponds almost exactly to a $Li:NH_3$ ratio of 1:4. Thus the $Li(NH_3)_4$ cluster is the simplest gas phase analog of a saturated lithium-ammonia solution. The nearest-neighbor distances determined from an analysis of the neutron diffraction data show a well-defined primary solvation shell.[44] The Li–N distance was found to be 2.06±0.02 Å, and the average coordination number of each Li atom was found to be 3.5. This Li–N distance is very similar to the Li–N distance in the lowest energy isomer of $Li(NH_3)_4$ obtained from the DFT calculations in the present work (2.093 Å). The neutron diffraction data confirm an approximately tetrahedral arrangement of four ammonia molecules around each atom. However, the observed N–N distances in this primary solvation shell were found to be inconsistent with a perfect tetrahedron, and were instead attributed to a distorted tetrahedron. Interestingly, this matches one of the interpretations of the IR spectrum of gas phase $Li(NH_3)_4$ given earlier; i.e., a single solvation shell structure occurs, but not with a perfect tetrahedral arrangement of the ammonia molecules around the lithium atom. Thus at face value the structural information from the saturated solution study seems to agree rather well with the gas phase spectroscopic data and *ab initio* calculations reported in the present work.

In saturated lithium-ammonia solutions virtually all of the ammonia molecules are locked into primary solvation shells and there is no possibility of any intershell hydrogen bonding. In more dilute solutions ammonia molecules located outside of the first solvation shell can now hydrogen bond to ammonia molecules in the first shell. Neutron diffraction studies of these more dilute solutions are challenging, but in a recent study Thompson *et al.* have completed a structural analysis of a solution with 8 mol % of lithium.[45] At this lower concentration there is clear evidence for a well-defined second solvation shell. The ammonia molecules in

TABLE I. Calculated dissociation energies (for removal of a single ammonia molecule) for $n=1-5$ clusters.

n[a]	DFT (this work)	MP2 (this work)	MP2 (Ref. 41)
1	4884	3973	4547
2	4657	3748	3977
3	4858	4314	4512
4	3347	3380	3358
5	1029	837	—

[a]Only the lowest energy isomer has been considered for each of the parent and fragment clusters. The dissociation energies include zero point energy corrections and have been adjusted for basis set superposition errors using the counterpoise correction.

this shell are located at an average distance of ~4 Å from the Li atom. Wasse and co-workers claim that the N atoms in the second shell reside along the faces and edges of the approximately tetrahedral primary shell. The calculations in this work for $Li(NH_3)_5$, which is the most "dilute" cluster we have investigated using *ab initio* calculations, are inconsistent with the interpretation of the neutron diffraction data. Although the distance between the Li atom and the second shell ammonia molecule in the 4+1 isomer is 4.18 Å, which is close to the neutron diffraction value, the calculations on $Li(NH_3)_5$ show that the second shell ammonia molecule has a clear preference to hydrogen bond to a single inner shell ammonia molecule, rather than partake in any shared arrangement with several inner shell ammonia molecules, as would be the case if it was bound to a face or an edge of the primary shell "tetrahedron." It would be interesting to explore this matter more fully with DFT calculations on larger clusters to see if the presence of multiple ammonia molecules in the second shell has any impact on the primary-secondary shell hydrogen bonding, but such calculations are likely to be complex and have not been attempted in the present study.

D. Photodissociation mechanism and cluster dissociation energies

It has been assumed in the interpretation of the infrared spectra that single photon infrared absorption is responsible for the depletion of signal in a given mass channel, rather than resonance-enhanced multiphoton dissociation (REMPD). If single photon absorption is the mechanism for the observed IR signals, the photon energy must exceed the Li–N binding energy for a specific cluster. On the other hand, if REMPD is responsible for the spectra, we would expect to be able to see IR spectra of clusters with $n \leqslant 3$, but no such spectra have been obtained. The most likely explanation is therefore that single photon excitation is operational and only the clusters with $n \geqslant 4$ possess a sufficiently weakly bound ammonia molecule to bring about cluster depletion.

To explore this further, the Li–N bond dissociation energies of the $n=1-5$ clusters have been calculated and are shown in Table I.[41] The calculations were performed using the supermolecule approach, i.e.,

$$D_0[Li(NH_3)_n] = E[NH_3] + E[Li(NH_3)_{n-1}] - E[Li(NH_3)_n],$$

where E represents the total energy of the cluster or fragment at equilibrium, including the zero point vibrational energy, and D_0 is the dissociation energy for loss of one ammonia molecule from a given cluster. Both DFT and MP2 calculations have been employed, and the counterpoise correction was utilized to remove the basis set superposition error. Only the lowest energy isomer has been considered in each case. Also included in Table I are the only other calculated dissociation energies for a series of $Li(NH_3)_n$ clusters, which was a MP2 study by Mierzwicki and Latajka using a 6-311 $+G(d,p)$ basis set.[42]

The results in Table I support the findings of the experiments. Although the calculated dissociation energy depends on the method and basis set employed, the trends are clear. For $n=1-3$ the dissociation energy is far in excess of the infrared photon energies used in the present work. On the basis of these findings, we would not expect to see any photodepletion spectra for $n=1-3$ clusters, which ties in with the experimental observations. Interestingly, $Li(NH_3)_4$ has a substantially reduced Li–N bond dissociation energy compared with its smaller cousins, despite the additional ammonia molecule entering the same inner solvation shell. This reduction in binding energy is presumably the result of increased steric hindrance, given that the shell is now full. The net effect is that the calculated bond dissociation energy for $n=4$ falls to a level which is very close to the energies of the photons absorbed in the experiment. Given the inherent approximations in the dissociation energy calculations, it is possible that the infrared photon energies exceed the true $Li(NH_3)_4$ dissociation energy. However, even if the bond dissociation energy is marginally higher than the infrared photon energy, a fraction of hot molecules in the gas expansion may possess an internal energy which, along with subsequent photon absorption, is sufficient to get them above the dissociation limit. We do not at this stage know which of these scenarios is correct, especially given that we have not been able to estimate the internal cluster temperatures resulting from our experiment. However, given that we see a similar degree of depletion for all four clusters ($n=4-7$), the most likely explanation is that the photon energy for $n=4$ is already sufficient for dissociation without any help from internal energy. In other words, the spectroscopic data point to a Li–N dissociation energy of $\leqslant 3200\ cm^{-1}$ for $Li(NH_3)_4$, which is the first experimental determination of this quantity.

Finally, we note that clusters with $n \geqslant 5$ will inevitably possess one or more much more weakly bound ammonia molecules in the second solvation shell. This is confirmed by the calculated dissociation energy for removing one ammonia molecule from the lowest energy isomer of $Li(NH_3)_5$, which lies well below the energies of the photons used in the present work. Thus for $n \geqslant 5$ single photon dissociation is undoubtedly responsible for the observed spectra.

V. CONCLUSIONS

Infrared spectra of alkali-solvent clusters as a function of size have been recorded for the first time. These spectra provide information that can be linked to cluster structures and,

in particular, the completion of the first solvation shell. The IR spectrum of $Li(NH_3)_4$ shows no evidence of any bands due to ammonia molecules lying outside of the first solvation shell. In contrast, $Li(NH_3)_5$, $Li(NH_3)_6$, and $Li(NH_3)_7$ all show the blueshifted absorption features characteristic of ammonia molecules in a second solvation shell. These data provide strong evidence that the first solvation shell of $Li(NH_3)_n$ clusters is full at $n=4$. This finding is consistent with conclusions reached from previous gas phase photoionization measurements, and it is also consistent with structural information extracted from diffraction studies of bulk lithium-ammonia solutions.

In addition to providing structural information, the spectra may also be sensitive to the unpaired electron density distribution across the cluster, in particular through the relative band intensities. However, extracting such information will probably require an improved treatment than that employed in the theoretical component of the present work, and it has therefore not been explored here. Indeed, a necessary precondition would be a set of more sophisticated calculations that can reliably map all of the accessible structural landscape available to each cluster. We hope that the experimental data presented here will stimulate serious theoretical effort to model the behavior of a variety of alkali-ammonia clusters.

Future spectroscopic work in our laboratory is now focusing on other alkali-solvent clusters as a first step on the way to studying a wider variety of uncharged solute-solvent clusters. We already have preliminary data for $Na(NH_3)_n$ clusters, and spectra of $Li(CH_3NH_2)_n$ clusters have also been recently recorded. The results of these and other related studies in progress will be published at a later date.

ACKNOWLEDGMENTS

The authors would like to thank the UK Engineering and Physical Sciences Research Council (EPSRC) for a grant which made this work possible. Computational aspects were supported through the EPSRC National Service for Computational Chemistry, which provided both software and hardware resources. Financial support of one of the authors through an EPSRC-funded DTA studentship, is also gratefully acknowledged.

[1] E. J. Hart and M. Anbar, *The Hydrated Electron* (Wiley, New York, 1970).
[2] D.-F. Feng and L. Kevan, Chem. Rev. (Washington, D.C.) **80**, 1 (1980).
[3] I. V. Hertel, C. Hüglin, C. Nitsch, and C. P. Schulz, Phys. Rev. Lett. **67**, 1767 (1991).
[4] C. Nitsch, C. P. Schulz, A. Gerber, W. Zimmermann-Edling, and I. V. Hertel, Z. Phys. D: At., Mol. Clusters **22**, 651 (1992).
[5] R. Takasu, K. Hashimoto, and K. Fuke, Chem. Phys. Lett. **258**, 94 (1996).
[6] R. Takasu, F. Misaizu, K. Hashimoto, and K. Fuke, J. Phys. Chem. A **101**, 3078 (1997).
[7] C. Stenbach and U. Buck, J. Chem. Phys. **122**, 134301 (2005).
[8] D. C. Sperry, A. J. Midey, J. L. Lee, J. Qian, and J. M. Farrar, J. Chem. Phys. **111**, 8469 (1999).
[9] S. G. Donnelly and J. M. Farrar, J. Chem. Phys. **98**, 5450 (1993).
[10] J. I. Lee, D. C. Sperry, and J. M. Farrar, J. Chem. Phys. **114**, 6180 (2001).
[11] M. Sanekata, F. Misaizu, and K. Fuke, J. Chem. Phys. **104**, 9768 (1996).
[12] R. Takusu, K. Nishikawa, N. Miura, A. Sabu, K. Hashimoto, C. P. Schulz, I. V. Hertel, and K. Fuke, J. Phys. Chem. A **105**, 6602 (2001).
[13] S. Yoshida, K. Daigoku, N. Okai, A. Takahata, A. Sabu, K. Hashimoto, and K. Fuke, J. Chem. Phys. **117**, 8657 (2002).
[14] C. T. Scurlock, S. H. Pullins, J. E. Reddic, and M. A. Duncan, J. Chem. Phys. **104**, 4591 (1996).
[15] Y. Abate and P. D. Kleiber, J. Chem. Phys. **122**, 084305 (2005).
[16] W. Y. Lu, T. H. Wong, Y. Sheng, A. T. Lytle, and P. D. Kleiber, J. Phys. Chem. A **107**, 984 (2003).
[17] J. Chen, Y. C. Cheng, and P. D. Kleiber, J. Chem. Phys. **106**, 77 (1997).
[18] J. M. Farrar, Int. Rev. Phys. Chem. **22**, 593 (2003).
[19] M. A. Duncan, Int. J. Mass. Spectrom. **200**, 545 (2000).
[20] C. J. Weinheimer and J. M. Lisy, J. Chem. Phys. **105**, 2938 (1996).
[21] T. D. Vaden, C. J. Weinheimer, and J. M. Lisy, J. Chem. Phys. **121**, 3102 (2004).
[22] C. J. Weinheimer and J. M. Lisy, Int. J. Mass Spectrom. Ion Process. **159**, 197 (1996).
[23] T. D. Vaden and J. M. Lisy, Chem. Phys. Lett. **408**, 54 (2005).
[24] T. D. Varden and J. M. Lisy, J. Phys. Chem. A **109**, 3880 (2005).
[25] T. D. Varden and J. M. Lisy, J. Chem. Phys. **123**, 074302 (2005).
[26] M. A. Duncan, Int. Rev. Phys. Chem. **22**, 407 (2003).
[27] N. R. Walker, R. S. Walters, and M. A. Duncan, New J. Chem. **29**, 1495 (2005).
[28] C. A. Woodward, M. P. Dobson, and A. J. Stace, J. Phys. Chem. **100**, 5605 (1996).
[29] R. R. Wright, N. R. Walker, S. Firth, and A. J. Stace, J. Phys. Chem. **105**, 54 (2001).
[30] L. Puškar and A. J. Stace, J. Chem. Phys. **114**, 6499 (2001).
[31] J. Miyawaki, K. Sugawara, H. Takeo, C. Dedonder-Lardeux, S. Martrenchard-Barra, C. Jouvet, and D. Solgadi, Chem. Phys. Lett. **302**, 354 (1999).
[32] J. Miyawaki and K.-I. Sugawara, J. Chem. Phys. **118**, 2173 (2003).
[33] J. Miyawaki, S. Djafari, K.-I. Sugawara, and H. Takeo, J. Chem. Phys. **118**, 8 (2003).
[34] C. Nitsch, C. Hüglin, I. V. Hertel, and C. P. Schulz, J. Chem. Phys. **101**, 6559 (1994).
[35] C. P. Schulz and C. Nitch, J. Chem. Phys. **107**, 9794 (1997).
[36] P. Brockhaus, I. V. Hertel, and C. P. Schulz, J. Chem. Phys. **110**, 393 (1999).
[37] S. Süzer and L. Andrews, J. Am. Chem. Soc. **109**, 300 (1987).
[38] A. Loutellier, L. Manceron, and J. P. Perchard, Chem. Phys. **146**, 179 (1990).
[39] T. E. Salter and A. M. Ellis, (unpublished)..
[40] M. J. Frisch, G. W. Trucks, H. B. Schlege *et al.*, GAUSSIAN 03, Revision C.02, Gaussian, Inc., Wallingford, CT, 2004.
[41] See EPAPS Document No. E-JCPSA6-124-010623 for structural parameters and total energies for clusters with $n=1-5$ from DFT and MP2 calculations. This document can be reached via a direct link in the online article's HTML reference section or via the EPAPS homepage (http://www.aip.org/pubservs/epaps.html).
[42] K. Mierzwicki and Z. Latajka, Chem. Phys. **265**, 301 (2001).
[43] K. Hashomoto and K. Morokuma, J. Am. Chem. Soc. **117**, 4151 (1995).
[44] J. C. Wasse, S. Hayama, N. T. Skipper, and H. E. Fischer, Phys. Rev. B **61**, 1993 (2000).
[45] H. Thompson, J. C. Wasse, N. T. Skipper, S. Hayama, D. T. Bowron, and A. K. Soper, J. Am. Chem. Soc. **125**, 2572 (2003).